Effect of iron on density and sound velocity of ringwoodite at high pressure and high temperature

lei liu[1], Fengxia sun[1], hong liu[1], li yi[1], Chaowen xu[2], Jianguo Du[3], xiaoyu gu[1], hanyu wang[1], and guangshu yang[4]

[1]institute of earthquake forecasting, CEA
[2]Institute of Earthquake Forecasting, China Earthquake Administration (CEA)
[3]Institute of Earthquake Forecasting, CEA
[4]Faculty of Land Resources Engineering, Kunming University of Science and Technology

November 23, 2022

Abstract

As the most enriched composition of the lower part of mantle transition zone, properties of bearing-Fe ringwoodite are important to deduce the composition and structure of the mantle. For understanding the properties of Fe-bearing ringwoodite under condition of the lower mantle transition zone, the density and seismic wave velocity (Vp and Vs) of ringwoodite with different Fe content (0, 12.5, 25, 50, and 100 at%) were calculated under 300-2000K and 0-26 GPa by forcefeild combined with molecular dynamic method. Changes of density, Vp and Vs of ringwoodite containing different Fe content with pressure and temperature were fitted by the binary linear equation. Density of ringwoodite linearly increases with increasing Fe content, however relationship between increase of Vp and Vs and increasing Fe content show quadratic. The calculated densities of ringwoodite show that the Fe content of ringwoodite shall be 55-64 at% to match the lower mantle transition zone's density. Therefor existence of ringwoodite may result in a low-density zone or gravity anomaly in the lower part of the mantle transition zone. The Vp and Vs of ringwoodite along the Earth's typical temperature and pressure profile are higher than the Earth's wave velocity model at the lower mantle transition zone (510-660 km) and the Vp and Vs of ringwoodite with 12.5 at% Fe along the Earth's typical temperature and pressure profile are 31.3-33.7%% and 22.9-27.7% higher. The calculated results provide new data to explore composition and structure of the mantle.

Supplementary Table 2.Sound velocity of ringwoodite with different Fe content under 300-1600K and 0-26GPa	Supplementary Table 2.Sound velocity of ringwoodite with different Fe content under 300-1600K and 0-26GPa	Supplementary Table 2.Sound velocity of ringwoodite with different Fe content under 300-1600K and 0-26GPa	Supplementary Table 2.Sound velocity of ringwoodite with different Fe content under 300-1600K and 0-26GPa	Supplementary Table 2.Sound velocity of ringwoodite with different Fe content under 300-1600K and 0-26GPa	Supplementary Table 2.Sound velocity of ringwoodite with different Fe content under 300-1600K and 0-26GPa	Supplementary Table 2.Sound velocity of ringwoodite with different Fe content under 300-1600K and 0-26GPa
T (K)	P (GPa)	Fe content (at%)	Fe content (at%)	Fe content (at%)	Fe content (at%)	Fe content (at%)
		0	12.5	25	50	100
Vs	**Vs**	**Vs**	**Vs**	**Vs**	**Vs**	**Vs**

300	0	5.93	5.82	5.74	5.59	5.10
500	0	5.86	5.75	5.68	5.53	5.07
800	0	5.75	5.65	5.58	5.42	5.01
1000	0	5.67	5.57	5.49	5.35	4.97
1100	0		5.53	5.45	5.31	4.94
1200	0	5.58	5.48	5.40	5.27	4.92
1400	0	5.49	5.38	5.32	5.19	4.87
1600	0	5.40	5.28	5.21	5.09	4.81
300	4	6.07	5.96	5.87	5.73	5.18
500	4	6.00	5.91	5.83	5.69	5.15
800	4	5.90	5.82	5.73	5.60	5.11
1000	4	5.83	5.75	5.67	5.53	5.07
1100	4	–	5.72	5.64	5.50	5.05
1200	4	5.76	5.69	5.60	5.46	5.03
1400	4	5.69	5.61	5.52	5.39	4.99
1600	4	5.61	5.54	5.45	5.33	4.94
300	8	6.16	6.08	5.98	5.83	5.26
500	8	6.11	6.03	5.94	5.78	5.23
800	8	6.03	5.96	5.86	5.71	5.19
1000	8	5.97	5.91	5.82	5.66	5.16
1100	8	-	5.88	5.79	5.64	5.14
1200	8	5.92	5.85	5.75	5.61	5.12
1400	8	5.87	5.80	5.70	5.56	5.09
1600	8	5.80	5.73	5.64	5.50	5.05
300	10	6.23	6.14	6.04	5.88	5.29
500	10	6.18	6.09	6.00	5.84	5.27
800	10	6.10	6.02	5.93	5.77	5.22
1000	10	6.05	5.97	5.88	5.72	5.20
1100	10		5.94	5.85	5.70	5.18
1200	10	6.00	5.91	5.83	5.67	5.16
1400	10	5.95	5.86	5.78	5.62	5.13
1600	10	5.89	5.80	5.72	5.57	5.10
1800	10	5.82	5.74	5.66	5.52	5.06
2000	10	5.76	5.68	5.60	5.46	5.03
300	12	6.28	6.18	6.08	5.92	5.31
500	12	6.23	6.14	6.04	5.88	5.29
800	12	6.17	6.07	5.98	5.82	5.26
1000	12	6.12	6.03	5.94	5.77	5.23
1100	12	–	6.00	5.91	5.75	5.21
1200	12	6.07	5.97	5.89	5.73	5.20
1400	12	6.02	5.93	5.83	5.68	5.17
1600	12	5.97	5.87	5.79	5.63	5.14
1800	12	5.92	5.82	5.73	5.58	5.11
2000	12	5.85	5.76	5.67	5.52	5.08
300	16	6.37	6.26	6.15	5.99	5.37
500	16	6.33	6.22	6.12	5.96	5.35
800	16	6.28	6.17	6.07	5.91	5.32
1000	16	6.23	6.13	6.03	5.87	5.29
1100	16	–	6.11	6.02	5.85	5.28
1200	16	6.19	6.09	5.99	5.83	5.27
1400	16	6.15	6.04	5.95	5.79	5.24

1600	16	6.10	5.99	5.91	5.75	5.22
1800	16	6.05	5.95	5.87	5.71	5.19
2000	16	6.00	5.91	5.82	5.66	5.16
300	18	–	6.31	6.20	6.03	5.39
500	18	–	6.27	6.17	6.00	5.37
800	18	–	6.21	6.11	5.94	5.34
1000	18	–	6.17	6.08	5.91	5.32
1100	18	–	6.16	6.06	5.90	5.31
1400	18	–	6.10	6.00	5.84	5.28
1600	18	–	6.06	5.96	5.81	5.25
1800	18	–	6.01	5.91	5.77	5.23
2000	18	–	5.97	5.87	5.73	5.21
300	20	–	6.35	6.26	6.08	5.42
500	20	–	6.32	6.23	6.04	5.40
800	20	–	6.26	6.17	5.99	5.37
1000	20	–	6.22	6.13	5.95	5.35
1100	20	–	6.20	6.11	5.94	5.34
1200	20	–	6.18	6.09	5.93	5.33
1400	20	–	6.14	6.05	5.89	5.31
1600	20	–	6.11	6.01	5.85	5.28
1800	20	–	6.07	5.96	5.82	5.27
2000	20	–	6.02	5.92	5.78	5.25
300	22	6.49	6.38	6.27	6.10	5.44
500	22	6.46	6.34	6.24	6.07	5.42
800	22	6.40	6.29	6.20	6.03	5.40
1000	22	6.36	6.26	6.17	6.00	5.38
1100	22		6.24	6.15	5.98	5.36
1200	22	6.33	6.23	6.13	5.96	5.36
1400	22	6.30	6.20	6.09	5.92	5.34
1600	22	6.26	6.15	6.06	5.89	5.32
1800	22	6.22	6.12	6.03	5.85	5.30
2000	22	6.18	6.08	5.99	5.82	5.28
300	26	6.56	6.46	6.35	6.17	5.48
500	26	6.53	6.43	6.32	6.14	5.47
800	26	6.47	6.38	6.27	6.09	5.44
1000	26	6.44	6.34	6.24	6.07	5.42
1100	26		6.33	6.22	6.05	5.41
1200	26	6.41	6.31	6.21	6.03	5.40
1400	26	6.38	6.28	6.17	6.00	5.38
1600	26	6.34	6.24	6.14	5.97	5.36
1800	26	6.30	6.20	6.10	5.93	5.34
2000	26	6.27	6.16	6.06	5.90	5.32
300	0	5.93	5.82	5.74	5.59	5.10
500	0	5.86	5.75	5.68	5.53	5.07
800	0	5.75	5.65	5.58	5.42	5.01
1000	0	5.67	5.57	5.49	5.35	4.97
1100	0	–	5.53	5.45	5.31	4.94
1200	0	5.58	5.48	5.40	5.27	4.92
1400	0	5.49	5.38	5.32	5.19	4.87
1600	0	5.40	5.28	5.21	5.09	4.81
Vp	**Vp**	**Vp**	**Vp**	**Vp**	**Vp**	**Vp**

300	0	10.50	10.35	10.25	10.06	9.20
500	0	10.34	10.20	10.11	9.89	9.09
800	0	10.08	9.95	9.85	9.65	8.92
1000	0	9.90	9.77	9.64	9.46	8.78
1100	0	9.80	9.68	9.56	9.37	8.72
1200	0	9.70	9.56	9.46	9.25	8.65
1400	0	9.49	9.36	9.27	9.06	8.51
1600	0	9.29	9.15	9.05	8.86	8.37
300	4	10.87	10.74	10.60	10.39	9.45
500	4	10.73	10.60	10.47	10.26	9.35
800	4	10.48	10.35	10.23	10.04	9.21
1000	4	10.31	10.20	10.08	9.88	9.09
1100	4	10.22	10.13	9.98	9.79	9.05
1200	4	10.14	10.04	9.91	9.69	8.99
1400	4	9.96	9.86	9.74	9.54	8.87
1600	4	9.78	9.69	9.57	9.36	8.75
300	8	11.20	11.04	10.89	10.64	9.72
500	8	11.05	10.91	10.77	10.52	9.62
800	8	10.83	10.73	10.58	10.34	9.47
1000	8	10.68	10.57	10.45	10.21	9.37
1100	8		10.50	10.37	10.15	9.32
1200	8	10.55	10.42	10.30	10.08	9.28
1400	8	10.39	10.29	10.15	9.95	9.17
1600	8	10.24	10.13	9.99	9.80	9.07
300	10	11.38	11.19	11.04	10.81	9.84
500	10	11.22	11.09	10.93	10.69	9.74
800	10	11.01	10.89	10.75	10.52	9.59
1000	10	10.88	10.76	10.62	10.38	9.50
1100	10		10.68	10.53	10.32	9.44
1200	10	10.75	10.62	10.47	10.24	9.39
1400	10	10.60	10.47	10.33	10.11	9.29
1600	10	10.44	10.32	10.18	9.95	9.19
1800	10	10.26	10.17	10.04	9.82	9.09
2000	10	10.10	10.02	9.88	9.69	9.00
300	12	11.51	11.34	11.21	10.97	9.94
500	12	11.37	11.22	11.08	10.85	9.85
800	12	11.17	11.04	10.91	10.66	9.72
1000	12	11.05	10.90	10.77	10.54	9.62
1100	12		10.83	10.70	10.48	9.56
1200	12	10.91	10.76	10.64	10.42	9.52
1400	12	10.79	10.62	10.48	10.27	9.42
1600	12	10.65	10.49	10.37	10.15	9.32
1800	12	10.49	10.36	10.23	10.01	9.23
2000	12	10.35	10.22	10.11	9.87	9.13
300	16	11.78	11.62	11.45	11.22	10.17
500	16	11.65	11.50	11.33	11.11	10.07
800	16	11.50	11.33	11.18	10.92	9.95
1000	16	11.37	11.20	11.05	10.81	9.85
1100	16		11.14	10.99	10.76	9.81
1200	16	11.25	11.08	10.94	10.70	9.77
1400	16	11.14	10.94	10.82	10.59	9.67

1600	16	11.01	10.82	10.71	10.48	9.57
1800	16	10.87	10.70	10.58	10.34	9.47
2000	16	10.76	10.58	10.46	10.24	9.38
300	18		11.73	11.59	11.32	10.26
500	18		11.62	11.49	11.23	10.17
800	18		11.45	11.30	11.04	10.04
1000	18		11.34	11.19	10.94	9.96
1100	18		11.28	11.14	10.89	9.90
1400	18		11.11	10.95	10.72	9.77
1600	18		10.99	10.84	10.59	9.68
1800	18		10.86	10.70	10.47	9.59
2000	18		10.73	10.59	10.34	9.50
300	20		11.87	11.71	11.47	10.37
500	20		11.75	11.60	11.37	10.28
800	20		11.58	11.44	11.19	10.16
1000	20		11.48	11.32	11.08	10.08
1100	20		11.42	11.27	11.04	10.03
1200	20		11.36	11.23	10.97	9.99
1400	20		11.24	11.12	10.85	9.91
1600	20		11.14	11.00	10.74	9.83
1800	20		11.01	10.85	10.62	9.74
2000	20		10.90	10.74	10.48	9.65
300	22	12.16	11.97	11.82	11.56	10.44
500	22	12.05	11.86	11.72	11.45	10.36
800	22	11.89	11.70	11.56	11.30	10.25
1000	22	11.77	11.61	11.46	11.20	10.18
1100	22		11.55	11.40	11.14	10.13
1200	22	11.67	11.50	11.35	11.10	10.09
1400	22	11.55	11.38	11.23	10.97	10.01
1600	22	11.43	11.27	11.13	10.87	9.93
1800	22	11.32	11.16	11.03	10.77	9.84
2000	22	11.20	11.04	10.91	10.67	9.76
300	26	12.40	12.24	12.06	11.78	10.65
500	26	12.28	12.12	11.97	11.69	10.57
800	26	12.14	11.97	11.80	11.53	10.46
1000	26	12.03	11.85	11.71	11.44	10.37
1100	26		11.81	11.65	11.38	10.34
1200	26	11.91	11.76	11.60	11.32	10.30
1400	26	11.81	11.64	11.49	11.22	10.21
1600	26	11.69	11.55	11.37	11.12	10.14
1800	26	11.57	11.42	11.26	11.01	10.06
2000	26	11.48	11.31	11.13	10.90	9.98

Hosted file

`supplementary table 1.docx` available at https://authorea.com/users/542440/articles/600956-effect-of-iron-on-density-and-sound-velocity-of-ringwoodite-at-high-pressure-and-high-temperature

Effect of iron on density and sound velocity of ringwoodite at high pressure and high temperature

Lei. Liu [a*], Fengxia. Sun [a] , Chaowen. Xu [a], Jianguo. Du [a], Li. Yi [a], Hong. Liu [a], Xxiaoyu. Gu [a], Hanyu. Wang [a], Gguangshu. Yang [b]

[a] *United Laboratory of High-Pressure Physics and Earthquake Science, Institute of Earthquake Forecasting, Key Laboratory of Earthquake Prediction, CEA, 100036, Beijing, China*

[b] *Faculty of Land Resources Engineering, Kunming University of Science and Technology, 650093, Kunming, Yunnan, China*

1. Introduction

Iron is abundantly enriched in the mantle, usually substitutes magnesium in mantle minerals (Zhang et al., 2019). It was found that the incorporation of iron in silicate minerals modifies their physical properties (Ganskow et al., 2010; Higo et al., 2006; Mao et al., 2006;). Compared with effect of temperature, the variation of iron concentration in the cold subducting slab at mantle transition zone was more likely to help explain the observed velocity anomalies (Ringwood and Irifune, 1988; Higo et al., 2006; Ganskow et al., 2010; Jacobsen et al., 2004; Okuda et al., 2019; Zhang et al., 2019). The occurrence state of iron in the deep Earth attracted much attentions (Muir

* Corresponding author: liulei@ief.ac.cn (L. Liu); 13888600582@163.com (G. Yang)

and Brodholt, 2020). Experiment found that the Fe-bearing bridgmanite ($(Mg_{0.85}Fe_{0.15})SiO_3$) lost Fe and disproportionate to a nearly Fe-free $MgSiO_3$ bridgmanite and Fe-rich phase H at 95-101GPa and 2200-2400K (Zhang et al., 2014). The experiments showed that Fe^{2+} in the deep magma ocean disproportionately forms Fe^{3+} and metallic iron at high pressures. It is reported that the reduced metallic iron sinks to the core and leaves an oxidized mantle that leads to the degasification of carbon dioxide and water from the mantle (Armstrong et al., 2019).

Ringwoodite is a high-pressure polymorph of olivine with the spinel-structured $(Mg,Fe)_2SiO_4$, and is considered to be the major constituent mineral of the Earth's mantle between depths of 510 and 660 km (Ringwood and Irifune, 1988). The pyrolitic mantle is mainly composed of ～60% ringwoodite and ～40% majoritic garnet at conditions of the lower part of the mantle transition zone (Hirose, 2002; Irifune, 1987). The velocity increase across the 410km, 520km and 660 km discontinuity may be caused by phase transition of olivine to its high pressure ploymorphs (wadsleyite, ringwoodite) respectively (Matsui, 2001). Iron content of ringwoodite is suggested to be 10 at% (Higo et al., 2008). Thus, the properties of Fe-bearing- ringwoodite under high pressure and high temperature are important to understand the structure and composition of the mantle. So knowledge of structural and thermoelastic properties of ringwoodite have been widely studied: thermal expansion at high-temperatures (Suzuki et al., 2009), room temperature compressibility (Hazen, 1993; Zerr et al., 1993), sound velocities at various pressures and temperatures (Weidner et al., 1984; Sinogeikin et al., 1997, 1998, 2001; Jackson et al., 2000; Katsura et al., 2004;Higo et al., 2004, 2006; Valdez et al., 2011, 2012; Rigden and Jackson, 1991; Rigden et al., 1991, 1992; Sinogeikin et al., 2001, Li et al., 2003). It is indicated that iron significantly affects the density and velocity of ringwoodite.

Theoretical calculations, e.g. the First-principle calculations, play a more effective role in studying material properties under the high pressure and temperature conditions because of rapid increasing of computational power. The First-principle methods are successfully used to simulate the Earth and planetary materials at high pressures and temperatures (Wentzcovitch and Stixrude, 2010; Jahn and Kowalski, 2014). Precisely determining effect of iron substitution on the physical properties of candidate mantle materials can provide critical insights into the composition and dynamics of the mantle (Lin et al., 2007; Lay et al., 2008). Studies on density and velocity of bearing-Fe ringwoodite under the simultaneously high-pressure and high-temperature conditions are still limited (Sinogeikin et al., 2003). Therefore, this work present the density and sound velocity of the ringwoodite with different Fe concentrations (0, 12.5, 25, 50, and 100 at%) under 0-26 GPa and 300-2000 K by the First-principle methods.

2. Simulated Method

The calculations were performed by the General Utility Lattice Program (GULP) codes (Gale and Rohl, 2003). The ClayFF forcefield was used to describe potential energy surface due to interactions between bonded atoms (Cygan et al., 2004). The ringwoodite is cubic and exists in a γ-spinel structure that belongs to space group Fd-3m and includes 56 atoms in its unit cell (Hazen et al., 1993). The 2×2×2 supercells are used in this work. The iron-bearing ringwoodites were constructed by substituting the magnesium in the pure-Mg phase with iron and 4 structures that contain 12.5, 25, 50 and 100 at% Fe were built. The molecular dynamic simulations were performed in the statistical ensemble of constant-pressure and constant temperature (NPT). The equilibrium time is 10 ps, the time step is 0.2 fs and the total production time is 100 ps for every calculation run.

3. Results

3.1 Benchmark calculations

The test calculations on lattice parameters and elastic properties of ringwoodite were carried out for assessing the performance of the forcefield combined with molecular dynamic approach used here. The calculated density (ρ), bulk modulus (K), shear modulus (G), compressional wave velocities (Vp), and shear wave velocities (Vs) are listed in Table 1 together with the previous data at ambient conditions for comparison.

Table 1 The density and elastic properties of ringwoodite at ambient condition

Composition	Density	K	G	Vp	Vs	Conditions	Reference
	g/cm^3	GPa		km/s			
Mg_2SiO_4	3.515	185	120	9.86	5.78	ambient	Li,et al., 2003
	3.515	184	120	9.75	5.82	ambient	Rigden,et al.,1991
		190	125	9.93	5.87	0GPa, 0K	Kiefer,et al.,1997
	3.559	185	120	9.85	5.82	ambient	Jackson,et al.,2000
	3.559	184	119	9.86	5.78	ambient	Weidner,et al.,1984
	3.572	185	127	9.96	5.93	ambient	Higo, et al., 2006
	3.61	196.5	124.7	10	5.9	0GPa, 0K	Nunez-Valdez, et al.,2011
	3.501	218.6	120.8	10.43	5.89	300K, 0GPa	This work
Mean differences (%)	-1.4%	+16.6%	-0.5%	+5.6%	+1.1%		
$(Mg_{0.91}Fe_{0.09})_2SiO_4$	3.69	186	119	9.66	5.68	ambient	Y.Higo,2008
	3.701	188.2	119.5	9.69	5.68	0.05GPa,295K	Sinogeikient, et al. 1998
	3.702	187.6	120.6	9.70	5.71	0GPa, 295K	Sinogeikient, et al. 2003
$(Mg_{0.75}Fe_{0.25})_2SiO_4$	3.878	193	113	9.39	5.4	ambient	Sinogeikient, et al.,1997
$(Mg_{0.5}Fe_{0.5})_2SiO_4$	4.176	191	102	8.85	4.94	ambient	Higo, et al., 2006
$(Mg_{0.875}Fe_{0.125})_2SiO_4$	3.70	197.1	120.5	9.7	5.6	0GPa, 0K	Nunez-Valdez, et al.,2011
	3.581	222.1	121.1	10.35	5.82	300K, 0GPa	This work
Mean differences (%)	-3.2%	+12.7%	-0.5%	+6.7%	+3.9%		

Our derived values of density, G and Vs are agreement well with previous results at ambient condition (Li, et al., 2003; Rigden,et al.,199; Kiefer,et al.,1997; Jackson, et al.,2000; Weidner, et al.,1984; Higo, et al., 2006, 2008; Nunez-Valdez, et al., 2011; Sinogeikient, et al., 1997, 1998, 2003), the mean difference are between 0.5% and 3.9%. The K and Vp, are respectively 5.6-6.7% and 12.7-16.6% larger than that of previous results.

To further verify validity of our used calculated approach, the density, Vp and Vs of ringwoodite with different Fe content under high pressure and temperature are also compared with previous results. The results are presented in Figure 1, 2 and 3.

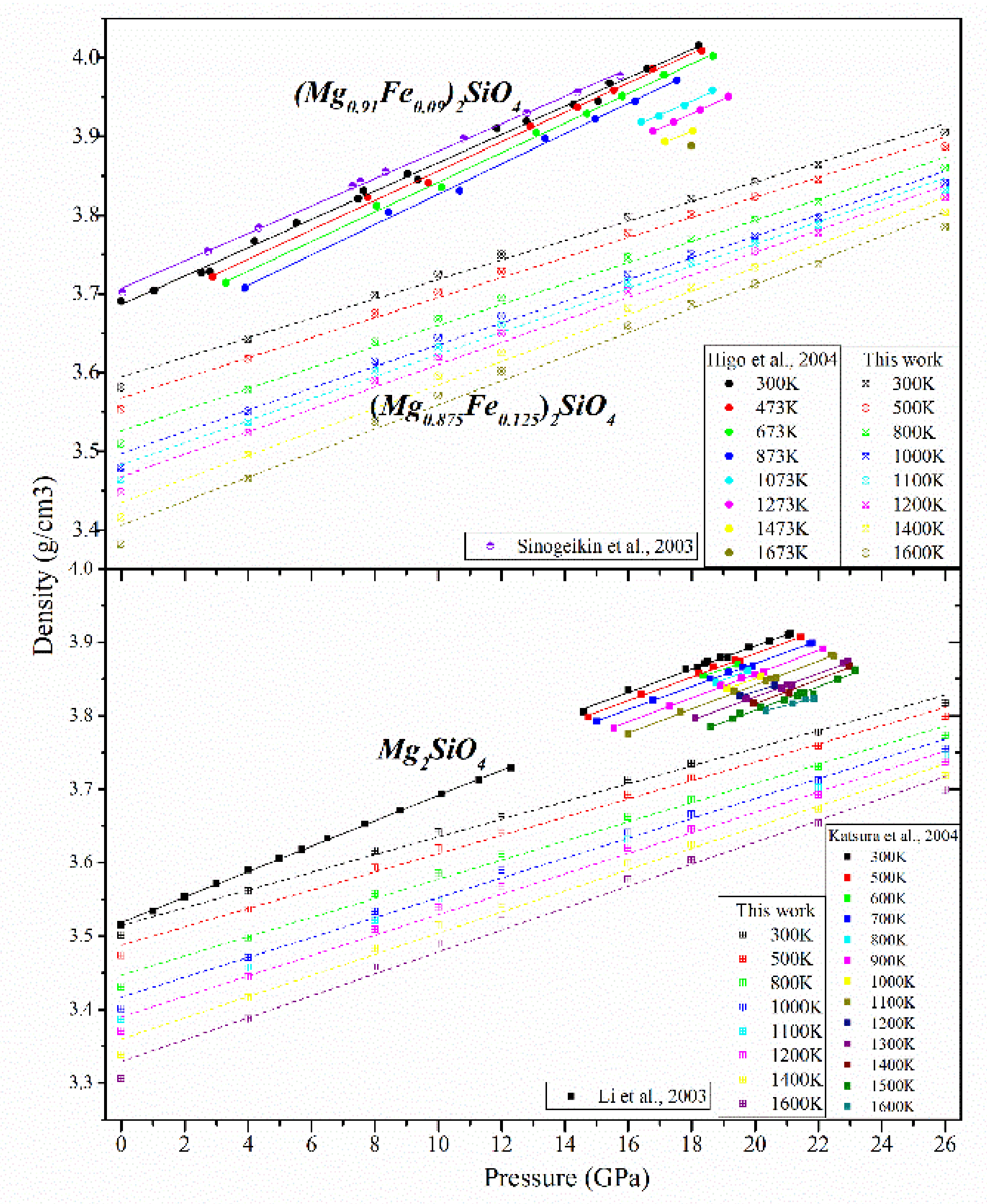

Figure 1. Density of ringwoodite with various Fe content at high pressure and temperature

Densities of Mg-endmember and Fe-bearing ringwoodite at 0-26 GPa and 300-1600K are shown in Figure 1. Higo et al. (2003) presented the density of ringwoodite with 10 wt% Fe. Our calculated densities are smaller than previous results up to 5.1% (Li et al., 2003; Sinogeikin et al., 2003; Katsura et al., 2004; Higo et al., 2004). The differences are slight in the low pressure and become larger with increasing pressure.

As shown in Figure 2 and 3, all our calculated velocities are larger than previous results (Jackson et al., 2000; Li et al., 2003; Higo et al., 2006; Valdez et al., 2012). The Vp and Vs of Mg-endmember ringwoodite is respectively ~ 6.8% and ~1.4% larger than the reported results of Li et al. (2003) and Higo et al. (2006) at 0-16 GPa and room temperature (Figure 2). Besides, the Vp and Vs of pure-Mg ringwoodtie is respectively ~ 5.2% and 1.1% larger than the reported results of Jackson et al. (2000) at 298-873K GPa and room pressure. Valdez et al. (2012) calculated Vp and Vs of pure-Mg ringwoodite at 0-30 GPa and 300-3000K by density functional theory (DFT) and quasiharmonic approximation (QHA) simulation (Figure 2). The velocity contrast ΔVp and ΔVs between ours and those reported by Valdez et al. (2012) is less than 10.2% and 8.1%, respectively.

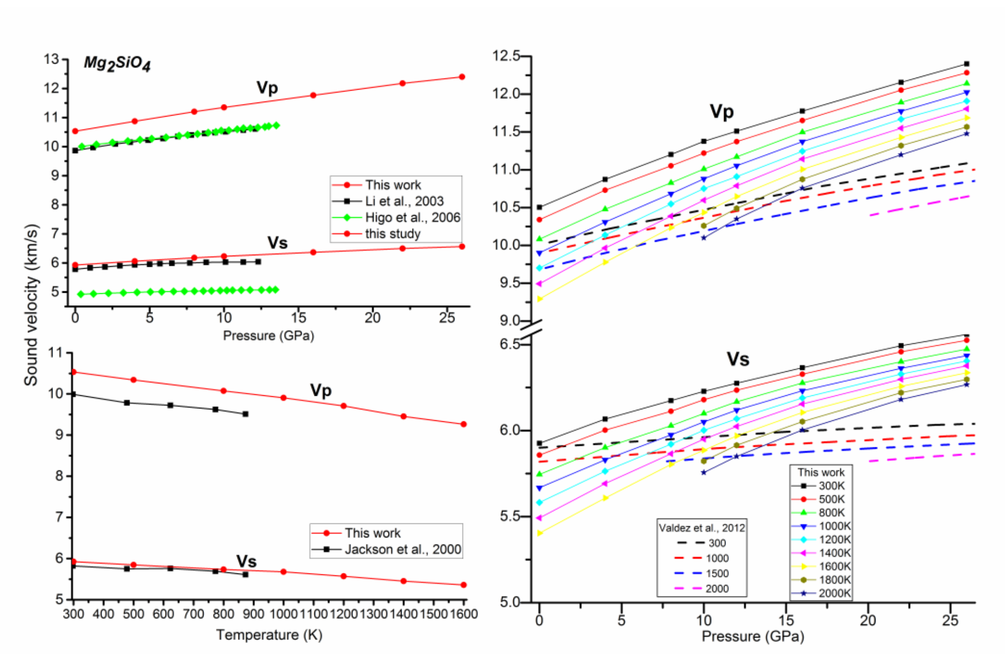

Figure 2 Comparison of velocity of Mg-endmember ringwoodite at high pressure and temperature

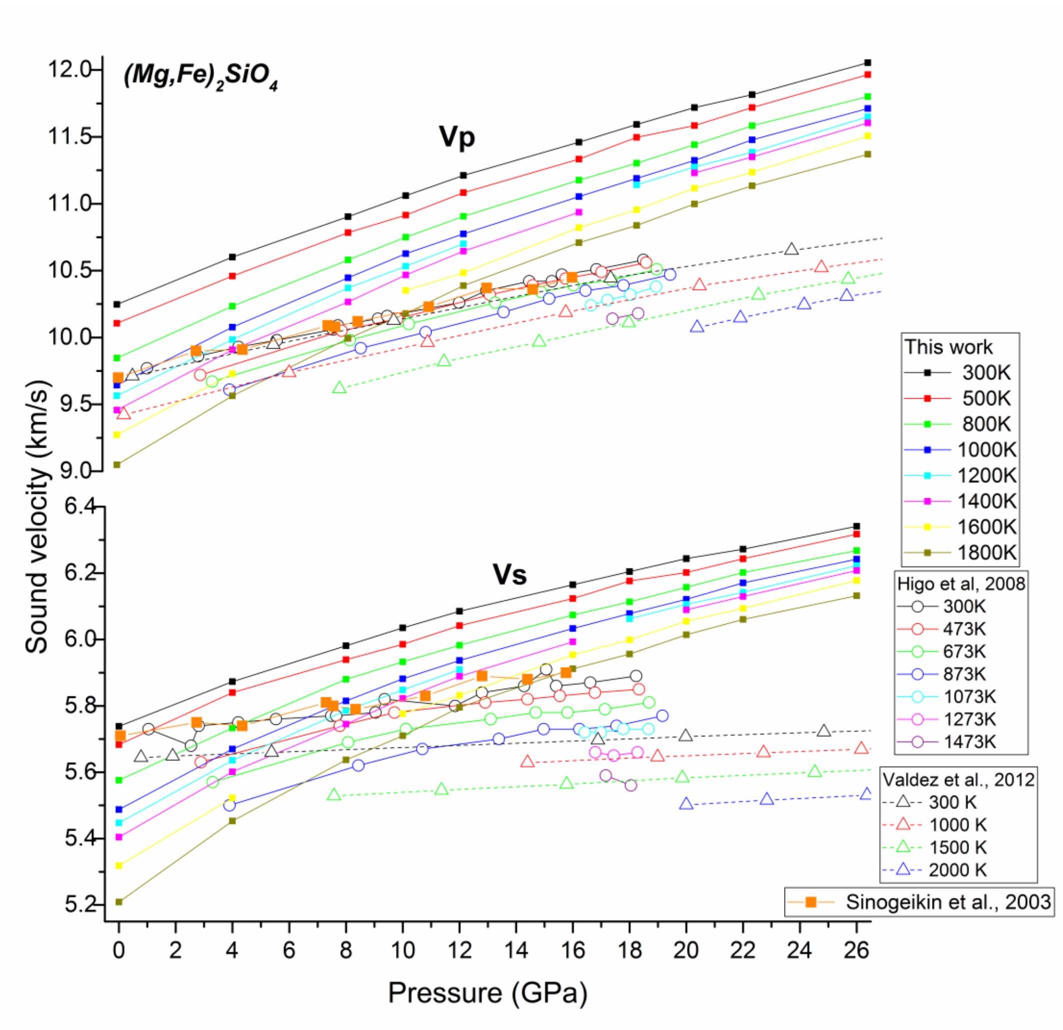

Figure 3 Comparison of velocity of Fe-bearing ringwoodite at high pressure and temperature

The comparisons of Vp and Vs of Fe-bearing ringwoodite with earlier studies are plotted in the Figure 3. Three works are used to be compared with our calculated $(Mg_{0.875}Fe_{0.125})_2SiO_4$ including the $(Mg_{0.875}Fe_{0.125})_2SiO_4$ (0-30 GPa and 300-3000K, Valdez et al., 2012), $(Mg0_{.91}Fe_{0.09})_2SiO_4$ (0-19.16 GPa and 300-1473K, Higo et al.,

2006) and $(Mg_{0.91}Fe_{0.09})_2SiO_4$ (0.05-15.76 GPa and room temperature, Sinogeikin, et al., 2003). The ΔVp and ΔVs between our calculated results and previous results (Valdez et al., 2012; Higo et al., 2006; Sinogeikin et al., 2003) increase with increasing pressure, up to 8.7% and 5.1%, respectively.

In general, compared with the previous results, our calculated values of density are smaller, K is larger, G is similar, and all Vp and Vs are larger. The biggest differences of density, Vp and Vs between our calculated results and previous results (Mg-endmember and Fe-bearing phase included) are 5.1%, 10.2% and 8.1% at range of 0-26 GPa and 300-2000K, respectively. At the same time, the differences increase with increasing pressure. Namely our calculated pressure gradients of density, Vp and Vs are larger than previous results. In a word, those results prove the validity of the calculated method used here for simulating the properties of ringwoodite under high pressure and high temperature.

3.2 The effect of Fe on density

Changes of the densities of ringwoodite with different Fe content under 0-26 GPa and 300-2000K are presented in Figure 4, Table 2 and supplementary table 1. The densities linearly increase with increasing Fe content and pressure; however linearly decrease with increasing temperature. The changes of density with pressure and temperature are fitted as follows:

$$\rho = \rho_0 + \boldsymbol{a}T + \boldsymbol{b}P,$$

where ρ and ρ_0 is the density (g/cm^3), P indicates pressure (GPa) and T indicates the temperature (K), and ***a*** and ***b*** are fitting coefficient. The fitted results are shown in Table 2.

Table 2.Fitted coefficient of changes of density of ringwoodite with different Fe content

Fe content (at%)	0	12.5	25	50	100
ρ_0	3.528	3.609	3.689	3.848	4.783
a	-0.00011	-0.000113	-0.000114	-0.000117	-0.000131
b	0.01353	0.01386	0.01414	0.01472	0.01748

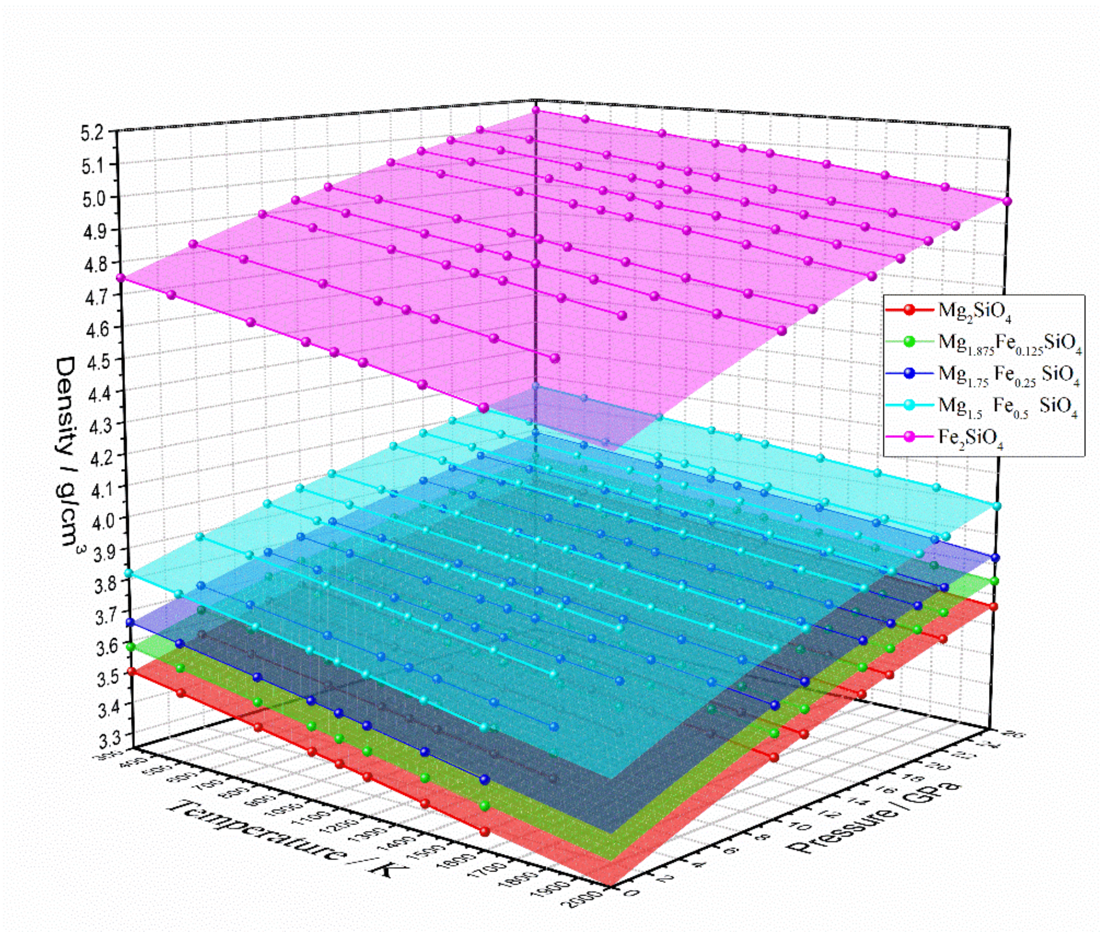

Figure 4 Densities of ringwoodite with different Fe content

To understand the quantitative effect of Fe, the comparison of Fe-bearing ringwoodite and Mg-endmember phase are shown in Figure 5. The differences between Fe-bearing ringwoodite and the Mg-endmember phase linearly increase with increasing Fe content. The fitted formula also listed in the Figure 5 under different pressure and temperature. The linear fitting coefficient decreases by 2.76% when temperature increasing from 300 K to 2000K, but increases by 8.19% when pressure increasing from 0 to 26 GPa.

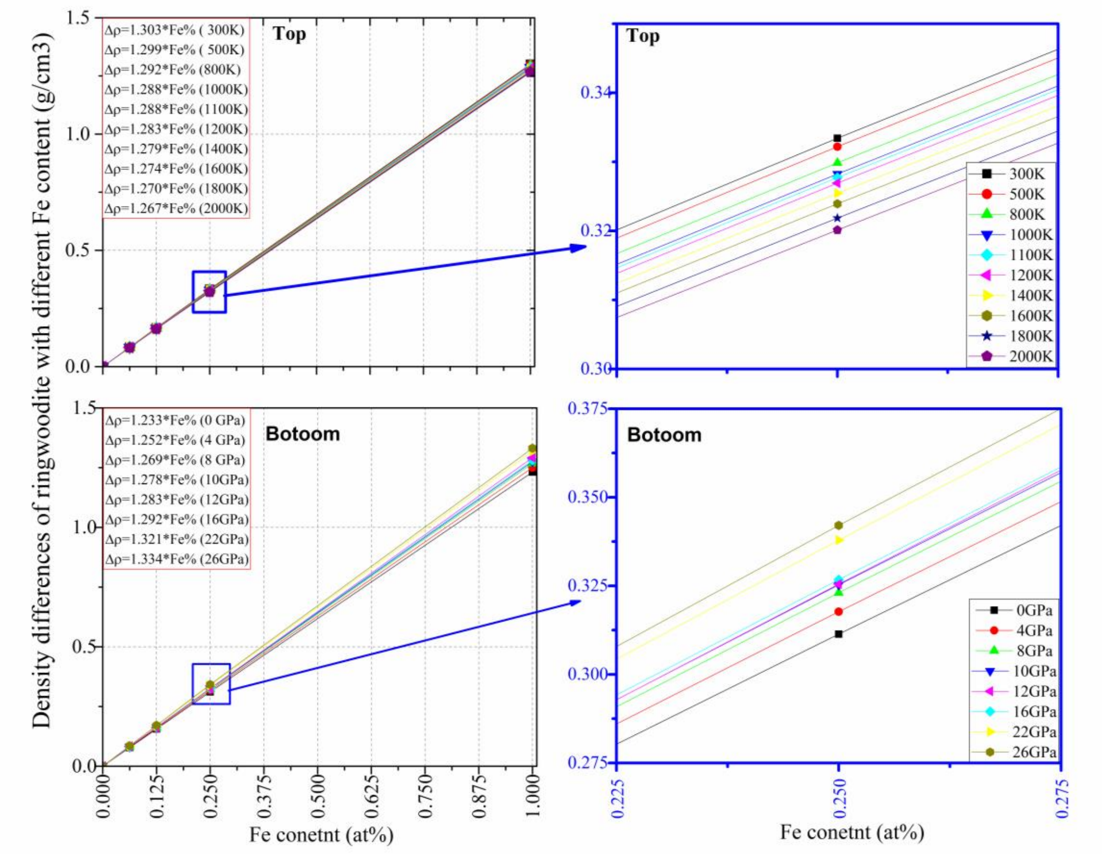

Figure 5 Differences of density of Fearing-ringwoodite with the Mg-endmember phase under different Fe condition

3.3 The effect of Fe on Vp and Vs

Vp and Vs of ringwoodite under 0-26 GPa and 300-2000K are presented in Figure 6 and supplementary table 2. Both Vp and Vs decrease with increasing temperature and Fe content, but increase with increasing pressure. The fitted results of Vp and Vs as a function of pressure and temperature are shown in Table 3. We notice that fitting coefficients slightly decrease with increasing Fe content.

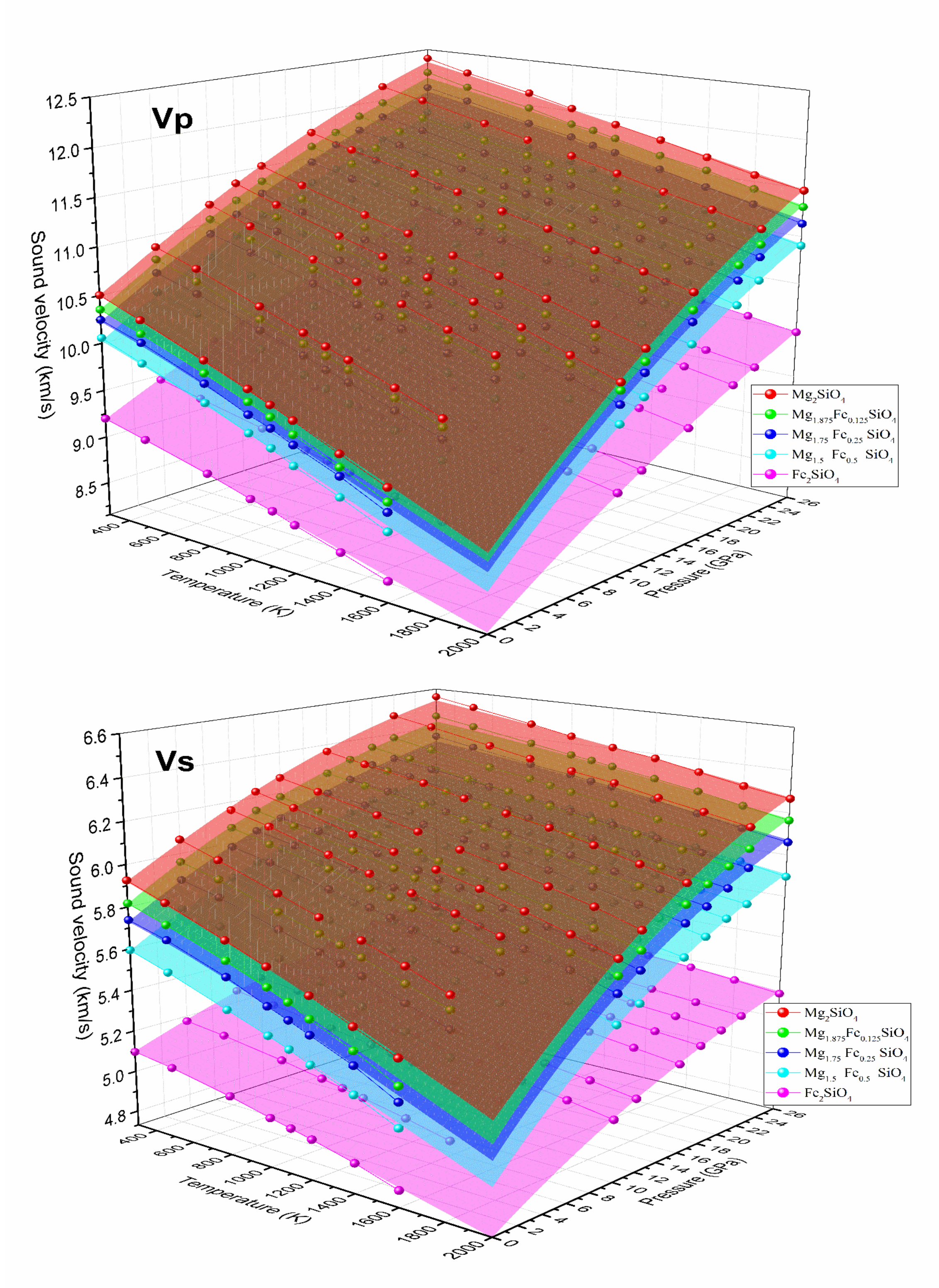

Figure 6 Sound velocity of ringwoodite with different Fe content under high pressure and temperature

Table 3. The fitted results of Vp and Vs as a function of pressure and temperature

Fe content (at%)	0	12.5	25	50	100
			Vp		
Vp_0	10.67	10.51	10.39	10.17	9.303
a	-0.000678	-0.000634	-0.000627	-0.000603	-0.000452
b	0.08184	0.07992	0.07837	0.07564	0.06099
			Vs		
Vs_0	5.963	5.858	5.772	5.624	5.122
a	-0.0002432	-0.0002264	-0.0002212	-0.0002091	-0.0001234
b	0.02998	0.02942	0.02856	0.02697	0.01746

Notes: The changes of Vp and Vs with pressure and temperature are fitted as follows: $V = V_0 + \boldsymbol{a}T + \boldsymbol{b}P$, where V and V_0 is the sound velocity (km/s), P indicates pressure (GPa) and T indicates the temperature (K), and ***a*** and ***b*** are fitting coefficient.

Changes of Vp and Vs (ΔVp and ΔVs) caused by variation of Fe content of ringwoodite are calculated by $(V_{Fe\text{-}bearing} - V_{Mg\text{-}endmember})/V_{Mg\text{-}endmember} \times 100\%$, where $V_{Fe\text{-}bearing}$ and $V_{Mg\text{-}endmember}$ indicate the V_P and Vs of Fe-bearing and Mg-endmember ringwoodite, respectively. The fitting results show well quadratic positive correlation and do not vary with pressure and temperature. The fitted results as follows:

$$\Delta Vp = 25.478 \times Fe\% - 11.238 \times (Fe\%)^2$$

$$\Delta Vs = 20.842 \times Fe\% - 10.807 \times (Fe\%)^2$$

where Fe% indicates the Fe content of ringwoodite with unit of at%.

Compared with Vp, Vs is more influenced by the Fe. For example, Vp and Vs of ringwoodite containing 12.5at% Fe are respectively 2.56% and 3.06% smaller than that velocity of Mg-endmember ringwoodite.

4. Discussion

As the most abundant constitute mineral of lower part of the mantle transition zone (Bass and Anderson, 1984; Hirose, 2002; Irifune, 1987), the density and sound velocity of ringwoodite are important to understand the composition and structure of the mantle, those properties are also useful to deduce the content of ringwoodite and Fe in the mantle.

According to above fitted results, the density of ringwoodite with different Fe content at lower part of the mantle transition zone conditions (along the Earth's temperature profile and pressure gradient) are plotted in Figure 7. The densities of Mg-endmember ringwoodite and those containing 12.5, 25 and 50 at% Fe are lower than that of the typical Earth's density profile (PREM; Dziewonski and Anderson, 1981), but the density of Fe-endmember ringwoodite is higher. On base of our calculation, the Fe content of ringwoodite is estimated to be 55-64 at% to match the density of lower part of the mantle transition zone. More Fe is needed to be incorporated in ringwoodite to meet the density profile of the lower mantle. Compared with experimental results, our calculated density is lower. This may lead to underestimate Fe content of ringwoodite that needed to match the Earth's density profile. Study showed that ringwoodite contains 10 at% Fe according to its low pressure polymorph of the San Carlos olivine with a composition of $(Mg_{0.91}Fe_{0.09})_2SiO_4$ (Higo et al., 2008). This content is much lower than that of 55-64%. Therefore, the existence of the ringwoodite may result in a low-density region or gravity anomaly in the lower part of the mantle transition zone (Chaves and Ussami, 2013; Bowin, 1983)

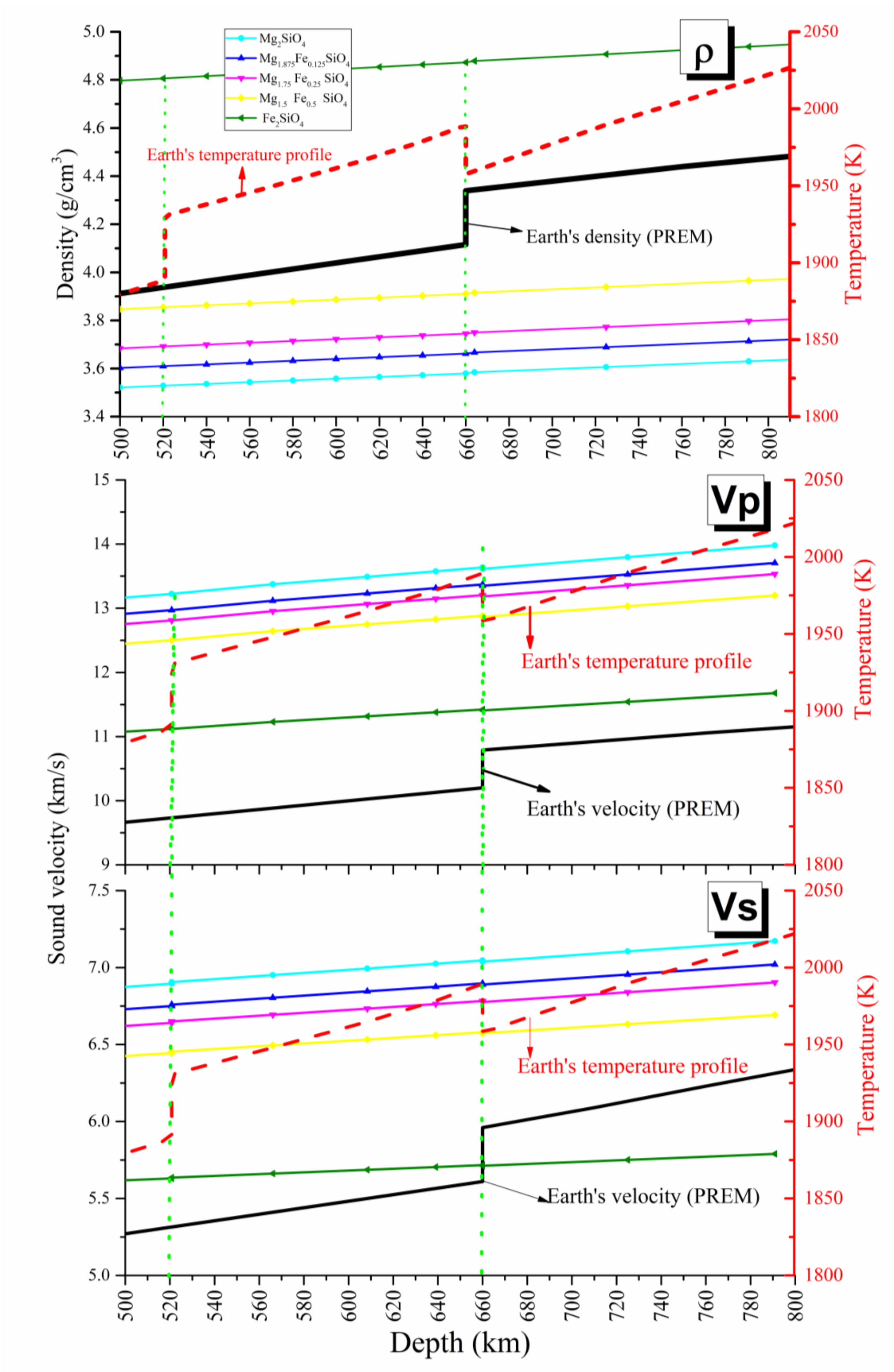

Figure 7 Density and sound velocity of ringwoodite along the Earth's temperature and pressure profile and comparison with the Earth's typical density model

The velocities obtained from seismic observation and those derived by experiments and calculations can reflect the composition and structure of the Earth. Thompson et al. (2017) showed that iron-enriched solid solutions in FeOOH-AlOOH-$MgSiH_2O_4$ system contribute to the observed large low-shear velocity provinces (LLSVP) in the lower mantle. Solid-state iron-enriched materials (Mao et al., 2006; Deng, et al., 2019; Muira and Brodholt, 2020) have been proposed to explain formation mechanism of the ultralow-velocity zones (ULVZs) at the core-mantle boundary. The wave velocities of ringwoodite with different Fe content under mantle transition zone condition are plotted in figure 7. The Vp and Vs of ringwoodite along the Earth's typical temperature and pressure profile are higher than that of the Earth's wave velocity model (Dziewonski and Anderson, 1981) at lower part of the mantle transition zone (510-660 km). The Vp and Vs of ringwoodite with 12.5 at% Fe content are 31.3-33.7% and 22.9-27.7% higher. Even for the pure-Fe ringwoodite, its Vp and Vs are still 12-14.7% and 1.9-6.5% higher. If ringwoodite can enter the lower mantle, the Vs of pure-Fe ringwoodite would lower than the PREM model, however the Vp of ringwoodite are still higher.

Ringwoodite will transform to bridgmanite+magnesiowüstite and then to post-pervoskite at the lower mantle condition (Murakami et al., 2004; Tsuchiya et al., 2004; Irifune et al., 1998; Ringwood, 1991). Experiment found that Fe-bearing bridgmanite ($(Mg_{0.85}Fe_{0.15})SiO_3$) lost Fe and disproportionated to a nearly Fe-free $MgSiO_3$ bridgmanite and an Fe-rich phase H at 95-101GPa pressure and 2200-2400K temperature (Zhang et al., 2014). Fe^{2+} ions in the deep magma ocean disproportionate to form Fe^{3+} ions and metallic iron at high pressures, and the reduced metallic iron sinks to the core and leaves an oxidized mantle that leads to the degasification of carbon dioxide and water from the mantle (Armstrong et al., 2019). Therefore Fe content and the properties of Fe-bearing ringwoodite is important to explore structure, composition and dynamic process of the mantle. Our calculated quantitative equations of Fe effect provide the information to constrain the Fe content of the deep Earth and help to understand the effect of Fe on evolution of the Earth.

5. Conclusion

The density,Vp and Vs of ringwoodite with different Fe content (0, 12.5, 25, 50, and 100 at%) under 300-2000K and 0-26 GPa were calculated by forcefeild combined with molecular dynamic method. This method is verified here to be effective in simulating physical properties of minerals. Changes of density, Vp and Vs of ringwoodite with pressure and temperature were fitted and presented. Density of ringwoodite linearly increases with increasing Fe content, however relationship between decrease of velocity and increasing Fe content show quadratic. Our calculated densities of ringwoodite show that the Fe content of ringwoodite shall be 55-64 at% to match the lower mantle transition zone's density. The existence of the ringwoodite may result in a low-density zone or gravity anomaly in the lower part of the mantle transition zone. The Vp and Vs of ringwoodite along the Earth's typical temperature and pressure profile are higher than the Earth's velocity. As the most important composition of lower mantle transition zone, the properties of Fe-bearing ringwoodite under high pressure and high temperature are significant to explore Fe content and composition of the mantle.

Acknowledgments

This work was supported by the Special Fund of the Institute of Earthquake Forecasting, China Earthquake Administration(Grant No. 2019IEF0101-1, 2019IEF0502, 2017KLEP03) and The Opening Foundation of the United Laboratory of High-Pressure Physics and Earthquake Science (Grant No. 2019HPPES06); and by the National Natural Science Foundation of China (Grant No.41762008). Datasets for this research are available in these in-text data citation references: Liu L., 2020. doi: 10.17632/xf2rktzfgw.1).

References:

1. Armstrong, K., McCammon, C.A., Rubie, D.C., Ballaran, T.B. (2019). Deep magma ocean formation set the oxidation state of Earth's mantle. *Science*, 365 (6456), 903-906.https://doi.org/10.1126/science.aax8376

2. Bowin, C. (1983). Depth of principal mass anomalies contributing to the earth's geoidal undulations and gravity anomalies. *Marine Geodesy*,7, 61–100. https://doi.org/10.1080/15210608309379476

3. Chaves, C.A.M., Ussami, N., (2013). Modeling 3-D density distribution in the mantle from inversion of geoid anomalies: Application to the Yellowstone Province. *Journal of Geophysical Research Solid Earth*, 118, 6328–6351.https://doi.org/10.1002/2013JB010168

4. Deng, J., Karki, B.B., Ghosh, D.B., Lee, K.K.M. (2019). First-principles study of FeO_2Hx

solid and melt system at high pressures: Implications for ultralow-velocity zones. *J. Geophys. Res. Solid Earth*, 124, 4566-4575 . https://doi.org/10.1029/2019JB017376

5. Dziewonski, A.M., Anderson, D.L. (1981). Preliminary Reference Earth Model (PREM). *Physics of the Earth & Planetary Interiors*, 25, 297-356. https://doi.org/10.1016/0031-9201(81)90046-7

6. Gale, J.D., Rohl, A.L. (2003). The general utility lattice program. *Molecular Simulation*, 29(5), 291-341. https://doi.org/10.1080/0892702031000104887

7. Ganskow, G., Ballaran, T.B., Langenhorst, F. (2010). Effect of iron on the compressibility of hydrous ringwoodite. *American Mineralogist*, 95, 747-753. https://doi.org/10.2138/am.2010.3420

8. Hazen, R.M., Downs. R.T., Finger, L.W., Ko. J. (1993).Crystal chemistry of ferromagnesian silicate spinels: Evidence for Mg-Si disorder, *American Mineralogist*, 78, 1320 - 1323. https://doi.org/doi:10.1016/0892-6875(93)90105-V

9. Hazen, R.M. (1993). Comparative compressibilities of silicate spinels: anomalous behavior of $(Mg, Fe)_2SiO_4$. *Science*, 259, 206-209. https://doi.org/10.1126/science.259.5092.206

10. Hazen, R.M., Weinberger, M.B., Yang, H., Prewitt, C.T. (2000). Comparative high pressure crystal chemistry of wadsleyite, β-$(Mg_{1-x}Fex)_2SiO_4$, with x=0 and 0.25, *American Mineralogist*, 85, 770-777. https://doi.org/10.2138/am-2000-5-617

11. Higo, Y., Inoue, T., Irifune, T., Funakoshi, K.I., Li, B. (2008). Elastic wave velocities of $(Mg_{0.91}Fe_{0.09})_2SiO_4$ ringwoodite under P-T conditions of the mantle transition region. *Physics of the Earth & Planetary Interiors*, 166, 167-174. https://doi.org/10.1016/j.pepi.2008.01.003

12. Higo, Y., Inoue, T., Li, B., Irifune, T., Liebermann, R. (2006). The effect of iron on the elastic properties of ringwoodite at high pressure. *Physics of the Earth & Planetary Interior*, 159, 276-285. https://doi.org/10.1016/j.pepi.2006.08.004

13. Hirose, K. (2002). Phase transitions in pyrolitic mantle around 670-km depth: implications for upwelling of plumes from the lower mantle. *Journal of Geophysical Research Solid*

Earth,107(B4), https://doi.org/10.1029/2001JB000597

14. Irifune, T. (1987). An experimental investigation of the pyroxene garnet transformation in a pyrolite composition and its bearing on the constitution of the mantle. *Physics of the Earth & Planetary Interiors*, 45, 324-336. https://doi.org/10.1016/0031-9201(87)90040-9

15. Irifune, T., Nishiyama, N., Kuroda, K., Inoue, T., Isshiki, M., Utsumi, W., Funakoshi, K., Urakawa, S., Uchida, T., Katsura, T., Ohtaka, O. (1998). The postspinel phase boundary in Mg2SiO4 determined by in situ X-ray diffraction. *Science*, 279, 1698-1700. https://doi.org/10.1126/science.279.5357.1698

16. Jackson, J.M., Sinogeikin, S.V., and Bass, J.D. (2000). Sound velocities and elastic properties of gamma-Mg_2SiO_4 to 873 K by Brillouin spectroscopy. *American Mineralogist*, 85, 296-303. https://doi.org/10.2138/am-2000-2-306

17. Jacobsen, S.D., Smyth, J.R., Spetzler, H., Holl, C.M., Frost, D.J. (2004). Sound velocities and elastic constants of iron bearing hydrous ringwoodite.*Physics of the Earth & Planetary Interiors*, 143, 47-56.18. https://doi.org/10.1016/j.pepi.2003.07.019

18. Jahn, S., Kowalski, P. (2014). Theoretical approaches to structure and spectroscopy of earth materials. *Reviews in Mineralogy & Geochemistry*, 78. https://doi.org/10.2138/rmg.2014.78.17

19. Katsura, T., Yokoshi, S., Song, M., Kawabe, K., Funakoshi, K. I. (2004). Thermal expansion of Mg_2SiO_4 ringwoodite at high pressures. *Journal of Geophysical Research Solid Earth*, 109(12), 221-232. https://doi.org/10.1029/2004JB003094

20. Kiefer, B., Stixrude, L., Wentzcovitch, R.M. (2013). Calculated elastic constants and anisotropy of Mg2SiO4 spinel at high pressure. *Geophys. Research Letters*, 24, 2841-2844. https://doi.org/10.1029/97GL02975

21. Komabayashi, T., Pesce, G., Sinmyo, R., Kawazoe, T., Breton, H., Shimoyama, Y. (2019). Phase relations in the system Fe-Ni-Si to 200 GPa and 3900 k and implications for earth's core. *Earth & Planetary Science Letters*, 512, 83-88.

https://doi.org/10.1016/j.epsl.2019.01.056

22. Lay, T., Hernlund, J., Buffett, B.A. (2008). Core-mantle boundary heat flow. *NATURE GEOENCE*, 1(1), 25-32. https://doi.org/10.1038/ngeo.2007.44

23. Li., Baosheng. (2003). Compressional and shear wave velocities of ringwoodite γ-mg2sio4 to 12 gpa. *American Mineralogist*, 88-89, 1312-1317. https://doi.org/10.2138/am-2003-8-913

24. Lin, J.F., Vanko, G., Jacobsen, S.D., Lota, V., Struzhkin, V.V., Prakapenka, V.B. (2007). Spin transition zone in earth's lower mantle. *Science*, 317(5845), 1740-1743. https://doi.org/10.1126/science.1144997

25. Núñez-Valdez. M., Wu. Z., Yu. Y.G., Revenaugh, J., Wentzcovitch. R.M. (2012). Thermoelastic properties of ringwoodite (Fex,Mg1−x)$_2$Sio$_4$: its relationship to the 520 km seismic discontinuity. *Earth & Planetary Science Letters*, 351-352.115-122. https://doi.org/10.1016/j.epsl.2012.07.024

26. Núñez-Valdez, M., da Silveira, P., Wentzcovitch, R.M. (2011). Influence of iron on the elastic properties of wadsleyite and ringwoodite.*Journal of Geophysical Research Solid Earth*, 116, B12207. https://doi.org/10.1029/2011JB008378

27. Mao, W.L., Mao, H.K., Sturhahn, W., Zhao, J., Prakapenka, V.B., Meng, Y. (2006). Iron-rich post-perovskite and the origin of ultralow-velocity zones. *Science*, 312(5773), 564-565. https://doi.org/10.1126/science.1123442

28. Mashino, I., Miozzi, F., Hirose, K., Morard, G., Sinmyo, R. (2019). Melting experiments on the fe-c binary system up to 255 GPa: constraints on the carbon content in the earth's core. *Earth & Planetary Science Letters*, 515, 135-144. https://doi.org/10.1016/j.epsl.2019.03.020

29. Matsui, M. (2001). Density and bulk sound velocity jumps across the 660 km seismic discontinuity. *Physics of the Earth & Planetary Interiors*, 125, 141-146. https://doi.org/10.1016/S0031-9201(01)00235-7

30. Murakami, M., Hirose, K., Kawamura, K., Sata, N., Ohishi, Y. (2004). Post-perovskite phase transition in $MgSiO_3$. *Science*, 304, 855-858. https://doi.org/10.1126/science.1095932

31. Muir, J.M.R., Brodholt, J.P. (2020). Ferric iron in bridgmanite and implications for ULVZs. *Physics of the Earth & Planetary Interiors*, 306, 106505. https://doi.org/10.1016/j.pepi.2020.106505

32. Okuda, Y., Ohta, K., Sinmyo, R., Takashi, K., Ohishi, Y. (2019). Effect of spin transition of iron on the thermal conductivity of (Fe, Al)-bearing bridgmanite. *Earth & Planetary Science Letters*, 520, 188-198. https://doi.org/10.1016/j.epsl.2019.05.042

33. Rigden, S.M., Gwanmesia, G.D., Fitz Gerald, J.D., Jackson, I., Liebermann, R.C. (1991). Spinel elasticity and seismic structure of the transition zone of the mantle. *Nature*, 354, 143-145. https://doi.org/10.1038/354143a0

34. Rigden, S.M., Gwanmesia, G.D., Jackson, I., Liebermann, R.C. (1992). Progress in high-pressure ultrasonic interferometry, the pressure dependence of elasticity of Mg2SiO4 polymorphs and constraints on the composition of the transition zone of the Earth's mantle. In: Syono, Y., Manghnani, M.H. (Eds.), High- Pressure Research: Application to Earth and Planetary Sciences. *American Geophysical Union*, *Washington, DC*, 167-182. https://doi.org/10.1029/GM067p0167

35. Rigden, S.M., Jackson, I. (1991). Elasticity of germanate and silicate spinels at high pressure. *Journal of Geophysical Research Solid Earth*, 96, 9999-10006. https://doi.org/10.1029/90JB02490

36. Ringwood, A.E. (1991). Phase transformations and their bearing on the constitution and dynamics of the mantle.*Geochimica et Cosmochimica Acta*, 55, 2083-2110. https://doi.org/10.1016/0016-7037(91)90090-R

37. Ringwood, A.E. and Irifune, T. (1988). Nature of the 650-km seismic discontinuity: implications for mantle dynamics and differentiation. *Nature*, 331(6152), 131-136. https://doi.org/10.1038/331131a0

38. Sinmyo, R., Hirose, K., Ohishi, Y. (2019). Melting curve of iron to 290 gpa determined in a resistance-heated diamond-anvil cell. *Earth & Planetary Science Letters*, 510, 45-52. https://doi.org/10.1016/j.epsl.2019.01.006

39. Sinogeikin, S.V., Bass, J.D., Katsura, T. (2003). Single-crystal elasticity of ringwoodite to high pressures and high temperatures: implications for 520 km seismic discontinuity. *Physics of the Earth & Planetary Interiors*, 136.1-2, 41-66. https://doi.org/10.1016/S0031-9201(03)00022-0

40. Sinogeikin, S.V., Bass, J.D., Katsura, T. (2001). Single-crystal elasticity of ɣ-$(Mg_{0.91}Fe_{0.09})_2SiO_4$ to high pressures and to high temperatures. *Geophysical Research Letters*, 28, 4335-4338. https://doi.org/10.1029/2001GL013843

41. Sinogeikin, S.V., Bass, J.D., Kavner, A., Jeanloz, R. (1997). Elasticity of natural majorite and ringwoodite from the Catherwood meteorite. Geophysical Research Letters, 24, 3265-3268. https://doi.org/10.1029/97GL03217

42. Sinogeikin, S.V., Katsura, T., Bass, J.D. (1998). Sound velocities and elastic properties of Fe-bearing wadsleyite and ringwoodite. *Journal of Geophysical Research Atmospheres*, 103, 20819-20825. https://doi.org/10.1029/98JB01819

43. Suzuki, I., Ohtani, E., Kumazawa, M. (2009). Thermal expansion of ɣ-Mg_2SiO_4. *Earth Planets & Space*, 27, 53-61. https://doi.org/10.4294/jpe1952.27.53

44. Tsuchiya, T., Tsuchiya, J., Umemoto, K., Wentzcovitch, R.M. (2004). Phase transition in $MgSiO_3$ perovskite in the Earth's lower mantle. *Earth & Planetary Science Letters*, 224, 241-248. https://doi.org/10.1016/j.epsl.2004.05.017

45. Weidner, D.J., Sawamoto, H., Sasaki, S., Kumazawa, M. (1984). Single-crystal elastic properties of the spinel phase of Mg_2SiO_4. *Journal of Geophysical Research Solid Earth*, 89, 7852-7860. https://doi.org/10.1029/JB089iB09p07852

46. Wentzcovitch R M , Stixrude L . Theoretical and computational methods in mineral physics : geophysical applications[M]. Mineralogical Society of America, 2010. https://doi.org/10.2138/rmg.2010.71

47. Zerr, A., Reichmann, H., Euler, H., Boehler, R. (1993). Hydrostatic compression of gamma-$(Mg_{0.6}$, $Fe_{0.4)2}SiO_4$ to 50.0 GPa. *Physics & Chemistry of Minerals*, 19, 507-509.

https://doi.org/10.1007/BF00203192

48. Zhang, L., Meng, Y., Yang, W. (2014). Disproportionation of (Mg,Fe)SiO_3 perovskite in Earth's deep lower mantle. *Science*, 344(6186), 877-882. https://doi.org/10.1126/science.1250274

49. Zhang, Y., Yoshino, T., Yoneda, A., Osako, M. (2019). Effect of iron content on thermal conductivity of olivine with implications for cooling history of rocky planets.*Earth & Planetary Science Letters*, 519, 109-119. https://doi.org/10.1016/j.epsl.2019.04.048

50. Zhang, B., Yoshino, T., Zhao, C. (2019). The effect of water on Fe-Mg interdiffusion rates in ringwoodite and implications for the electrical conductivity in the mantle transition zone. *Journal of Geophysical Research Solid Earth*, 124, 2510-2524. https://doi.org/10.1029/2018JB016415

Figure 1.

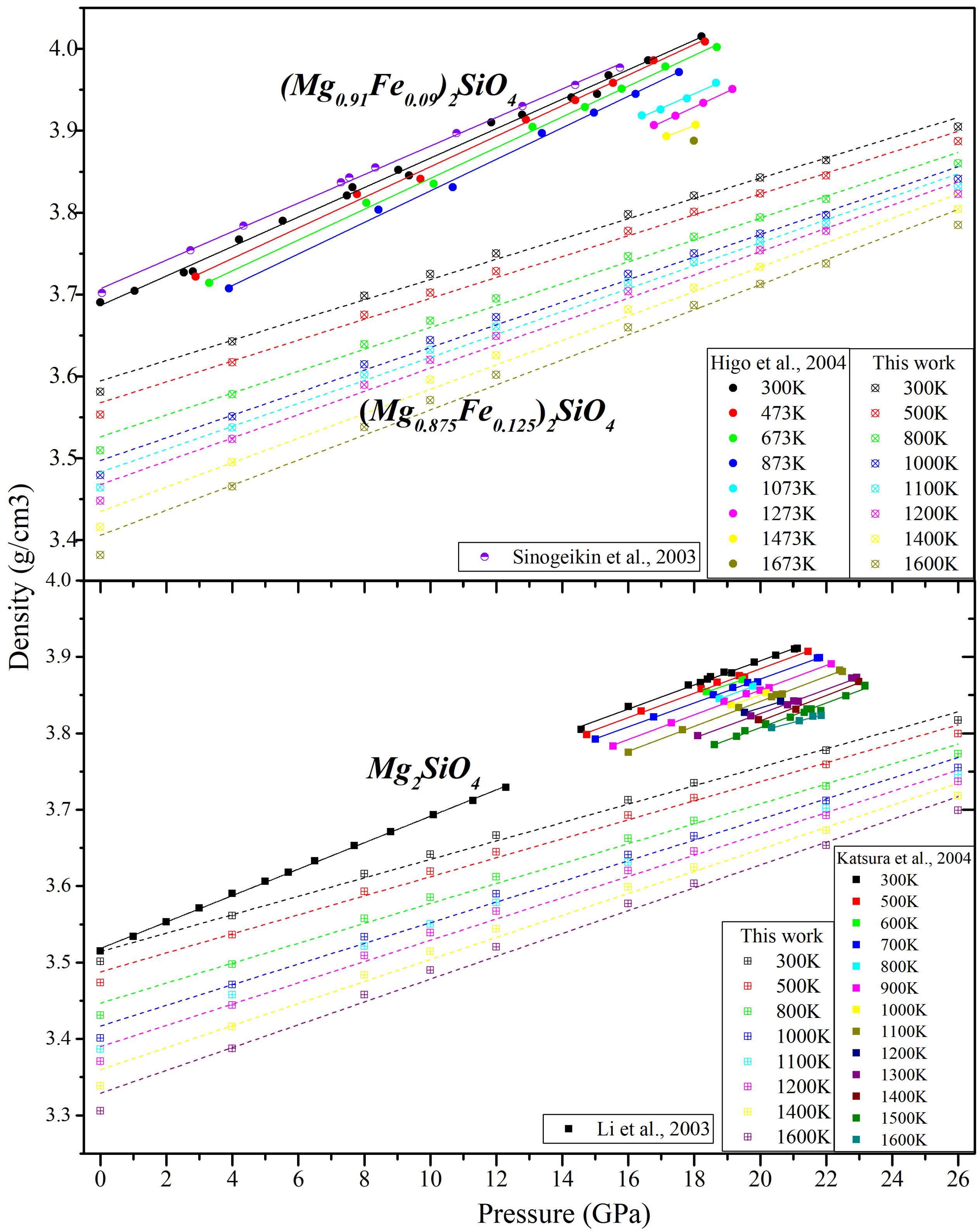

$(Mg_{0.91}Fe_{0.09})_2SiO_4$
$(Mg_{0.875}Fe_{0.125})_2SiO_4$
Higo et al., 2004
300K
473K
673K
873K
1073K
1273K
1473K
1673K
This work
300K
500K
800K
1000K
1100K
1200K
1400K
1600K
Sinogeikin et al., 2003
Mg_2SiO_4
Katsura et al., 2004
300K
500K
600K
700K
800K
900K
1000K
1100K
1200K
1300K
1400K
1500K
1600K
This work
300K
500K
800K
1000K
1100K
1200K
1400K
1600K
Li et al., 2003
Density (g/cm3)
Pressure (GPa)

Figure 2.

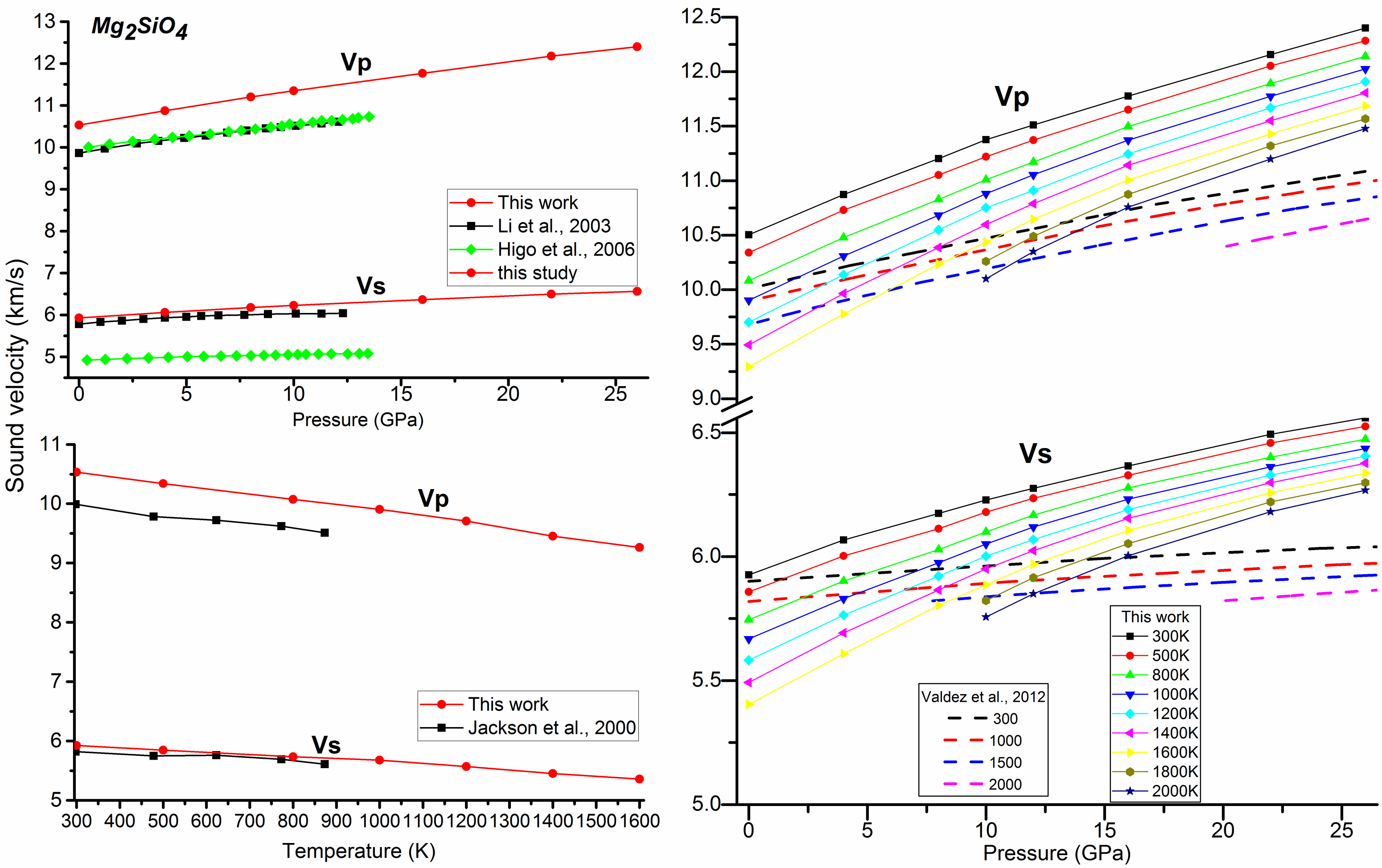

Mg2SiO4
Vp
Vs
This work
Li et al., 2003
Higo et al., 2006
this study
Pressure (GPa)
Sound velocity (km/s)
Jackson et al., 2000
Temperature (K)
Valdez et al., 2012
300
1000
1500
2000
This work
300K
500K
800K
1000K
1200K
1400K
1600K
1800K
2000K

Figure 3.

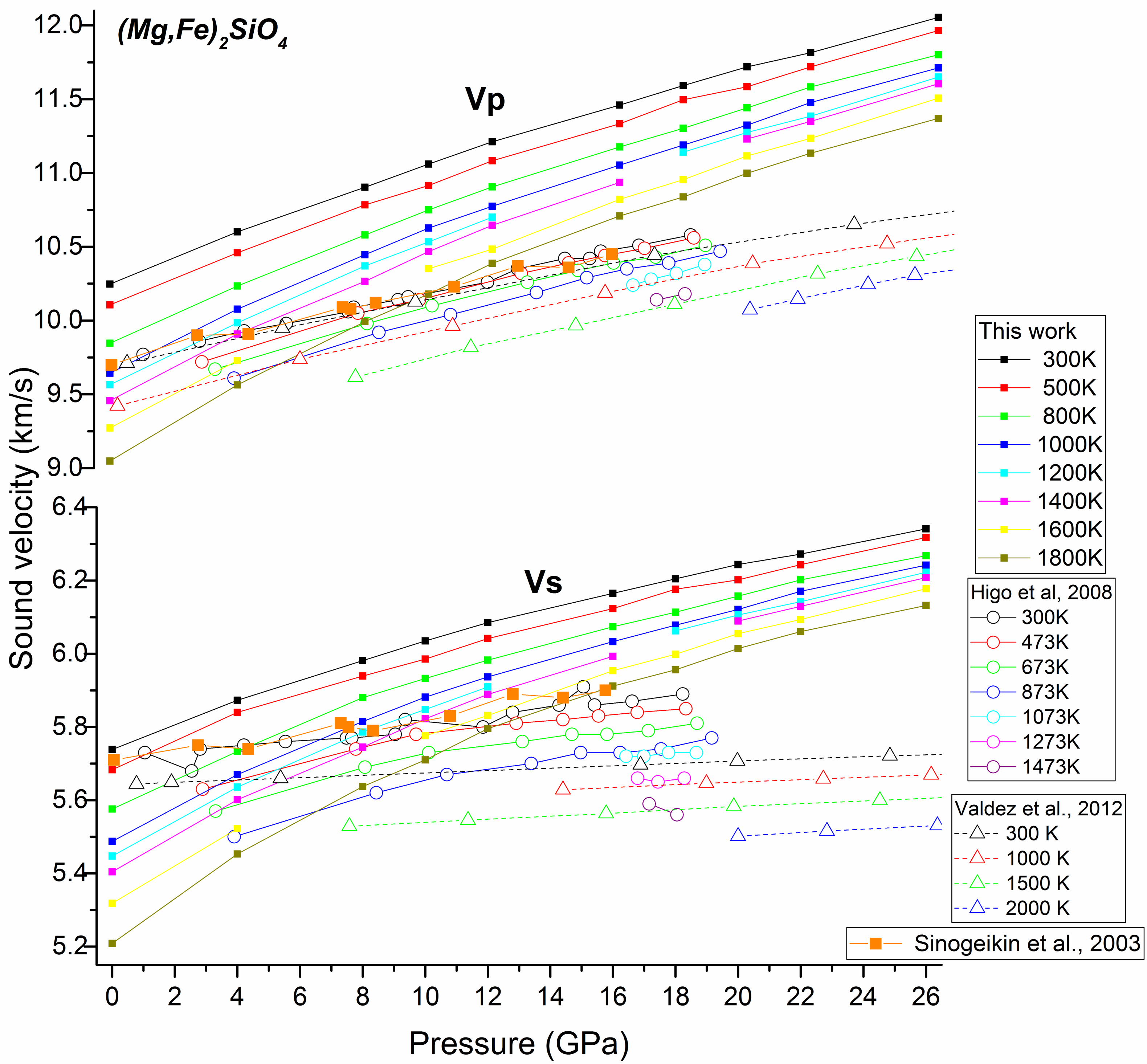

(Mg,Fe)$_2$SiO$_4$
Vp
Vs
Sound velocity (km/s)
Pressure (GPa)
This work
300K
500K
800K
1000K
1200K
1400K
1600K
1800K
Higo et al, 2008
300K
473K
673K
873K
1073K
1273K
1473K
Valdez et al., 2012
300 K
1000 K
1500 K
2000 K
Sinogeikin et al., 2003

Figure 4.

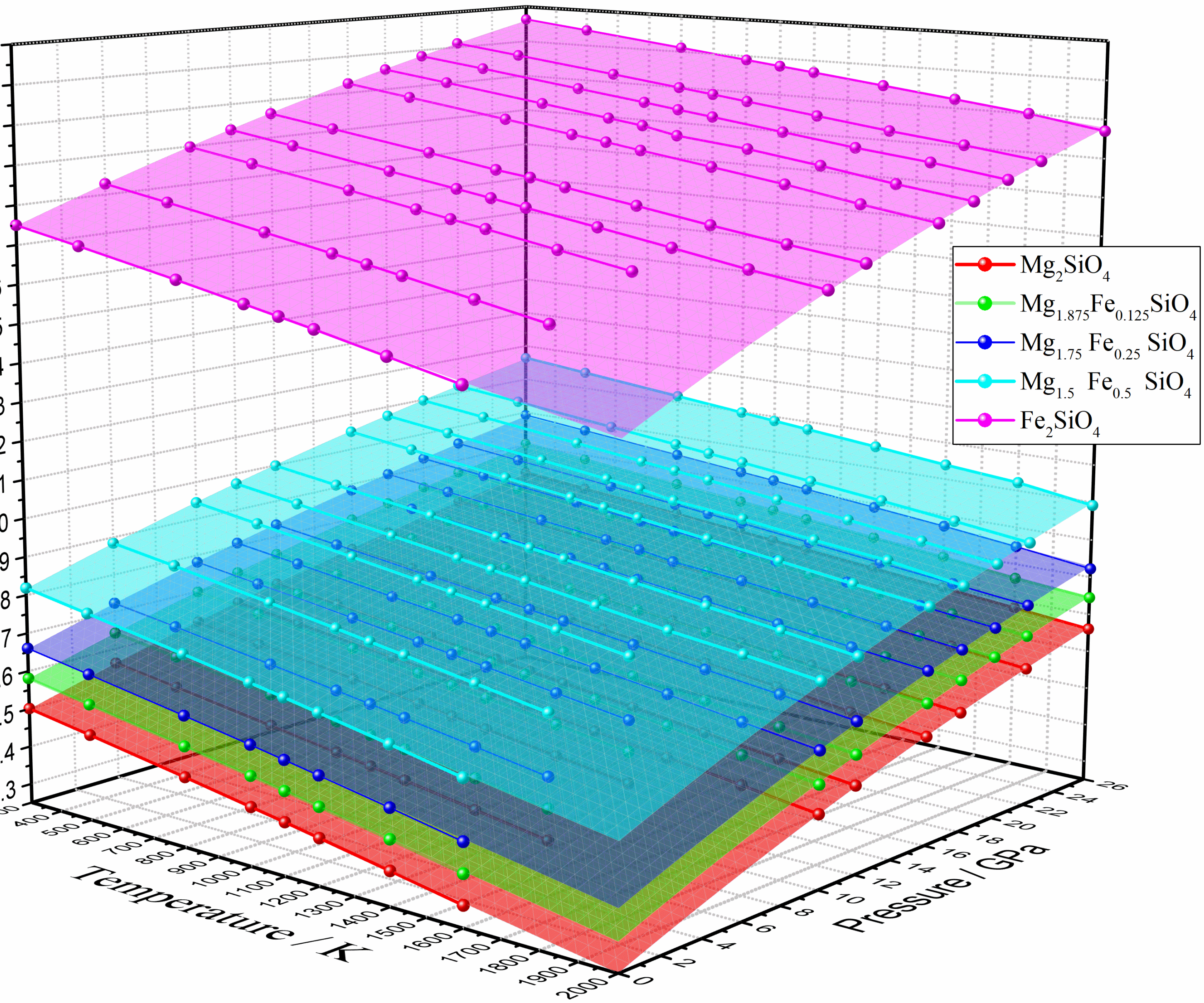
Density / g/cm^3
Temperature / K
Pressure / GPa
Mg_2SiO_4
$Mg_{1.875}Fe_{0.125}SiO_4$
$Mg_{1.75}Fe_{0.25}SiO_4$
$Mg_{1.5}Fe_{0.5}SiO_4$
Fe_2SiO_4

Figure 5.

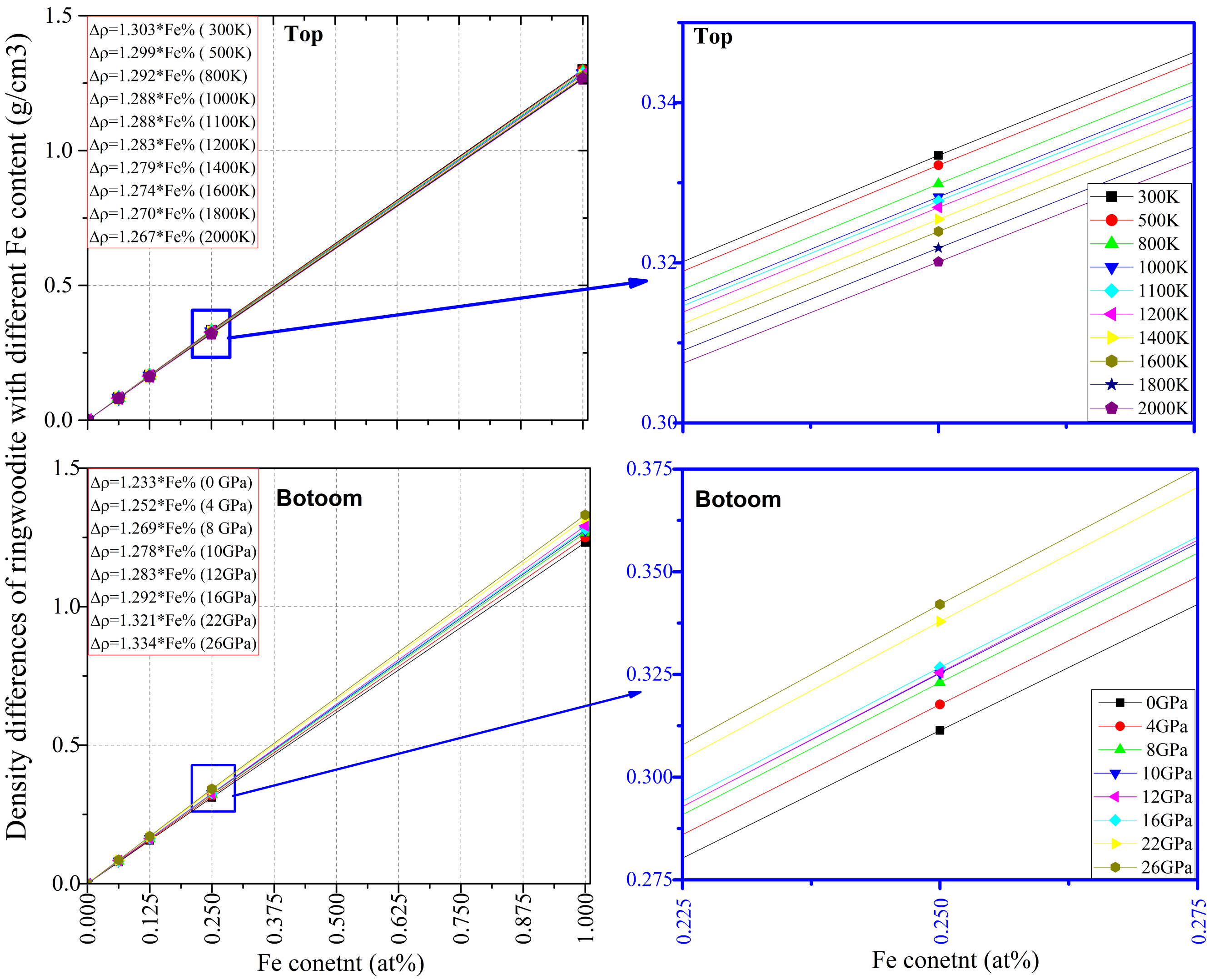

Density differences of ringwoodite with different Fe content (g/cm3)
Top
Δρ=1.303*Fe% (300K)
Δρ=1.299*Fe% (500K)
Δρ=1.292*Fe% (800K)
Δρ=1.288*Fe% (1000K)
Δρ=1.288*Fe% (1100K)
Δρ=1.283*Fe% (1200K)
Δρ=1.279*Fe% (1400K)
Δρ=1.274*Fe% (1600K)
Δρ=1.270*Fe% (1800K)
Δρ=1.267*Fe% (2000K)
300K
500K
800K
1000K
1100K
1200K
1400K
1600K
1800K
2000K
Botoom
Δρ=1.233*Fe% (0 GPa)
Δρ=1.252*Fe% (4 GPa)
Δρ=1.269*Fe% (8 GPa)
Δρ=1.278*Fe% (10GPa)
Δρ=1.283*Fe% (12GPa)
Δρ=1.292*Fe% (16GPa)
Δρ=1.321*Fe% (22GPa)
Δρ=1.334*Fe% (26GPa)
0GPa
4GPa
8GPa
10GPa
12GPa
16GPa
22GPa
26GPa
Fe conetnt (at%)
Fe conetnt (at%)

Figure 6.

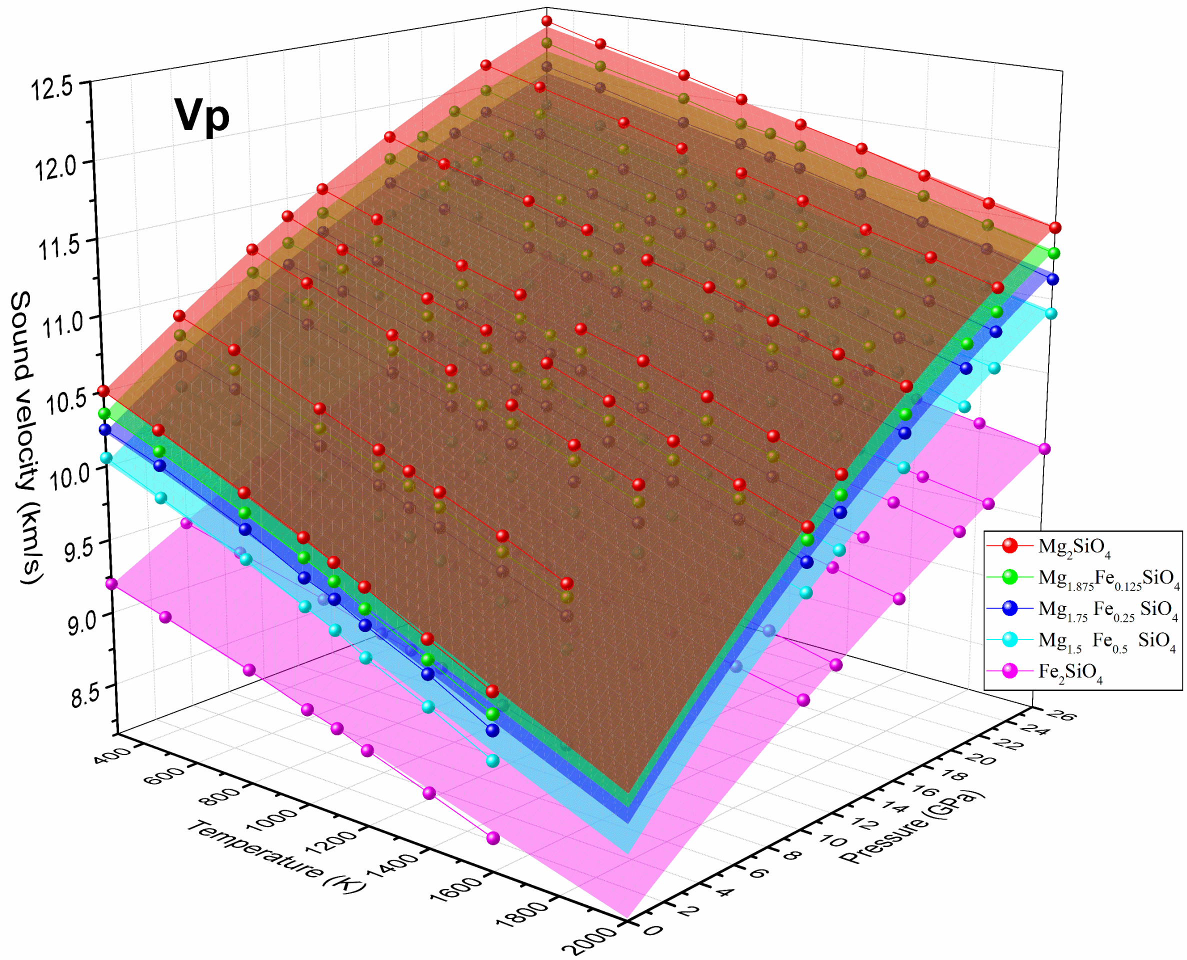
Vp
Sound velocity (km/s)
Temperature (K)
Pressure (GPa)
Mg_2SiO_4
$Mg_{1.875}Fe_{0.125}SiO_4$
$Mg_{1.75}Fe_{0.25}SiO_4$
$Mg_{1.5}Fe_{0.5}SiO_4$
Fe_2SiO_4

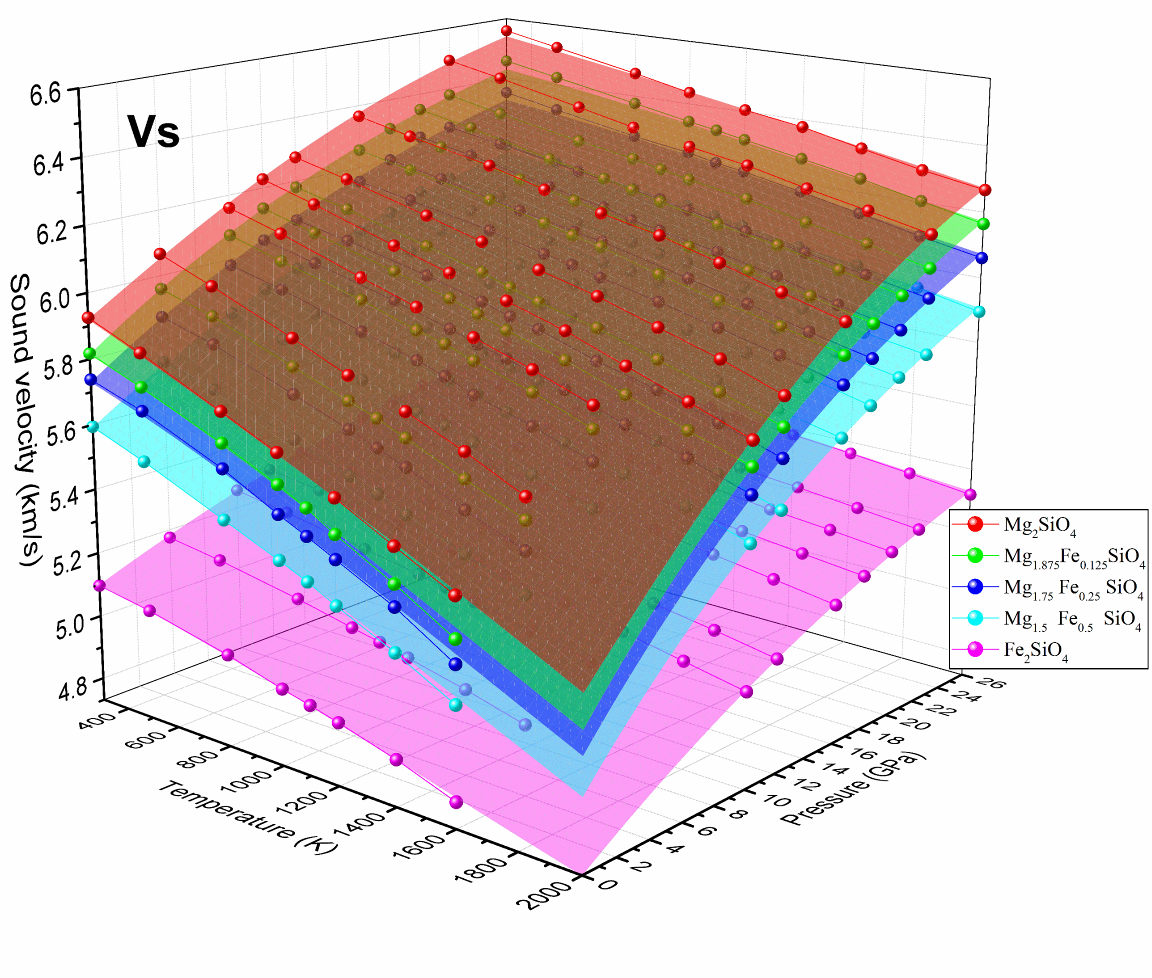
Vs
Sound velocity (km/s)
Temperature (K)
Pressure (GPa)
Mg_2SiO_4
$Mg_{1.875}Fe_{0.125}SiO_4$
$Mg_{1.75}Fe_{0.25}SiO_4$
$Mg_{1.5}Fe_{0.5}SiO_4$
Fe_2SiO_4

Figure 7.

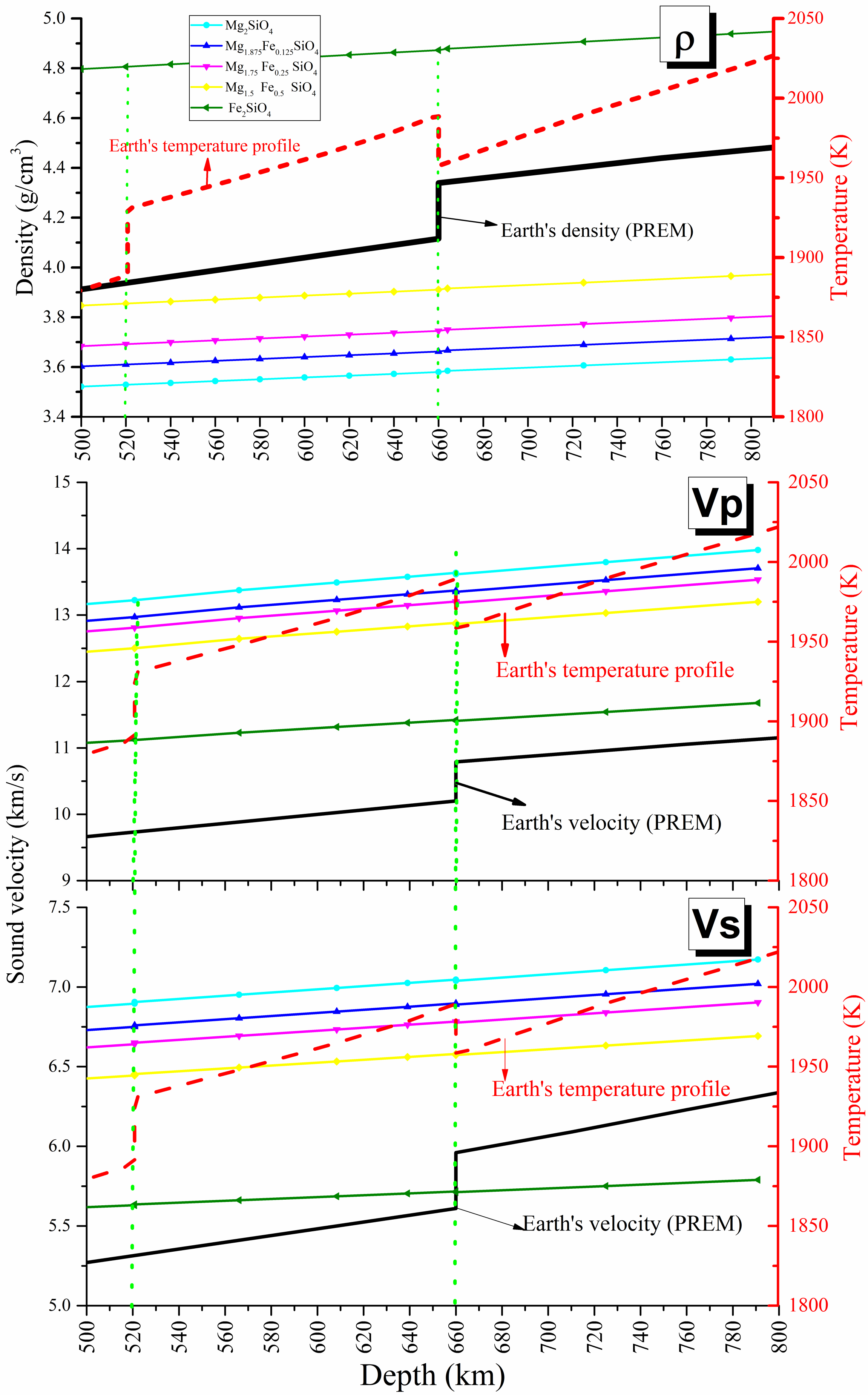

ρ
Vp
Vs
Mg2SiO4
Mg1.875Fe0.125SiO4
Mg1.75 Fe0.25 SiO4
Mg1.5 Fe0.5 SiO4
Fe2SiO4
Earth's temperature profile
Earth's density (PREM)
Earth's velocity (PREM)
Density (g/cm3)
Sound velocity (km/s)
Temperature (K)
Depth (km)